ASTFE
American Society
of Thermal and Fluids Engineers

7th Thermal and Fluids Engineering Conference (TFEC)
May 16-18, 2022
Partially Online Virtual and in Las Vegas Conference

TFEC-2022-40925

OPTIMIZATION METHODS FOR SEGMENTED THERMOELECTRIC GENERATORS

Shane P. Riley,[1] Sarah E. Wielgosz,[1] Kevin Yu,[2] Michael J. Durka,[2] Bill J. Nesmith,[2] Fivos Drymiotis,[2] Jean-Pierre Fleurial,[2] Matthew M. Barry[1,*]

[1]Department of Mechanical Engineering and Materials Science,
University of Pittsburgh, Pittsburgh, PA 15261, USA
[2]Jet Propulsion Laboratory, California Institute of Technology,
4800 Oak Grove Drive, Pasadena, CA 91109, USA

ABSTRACT

Future National Aeronautics and Space Administration deep-space missions are seeking radioisotope propulsion systems (RPS) to have specific powers above 8 [W_e/kg], while having thermal conversion efficiencies greater than 12%. The design and optimization of segmented thermoelectric unicouples used within RPS requires a multi-faceted approach to maximize device performance. The design space of a unicouple can span multiple dimensions, requiring immense computational resources to conduct parametric studies. These dimensions include, but are not limited to, the independent cross-sectional areas of the n- and p-type legs, the total height of the unicouple, the length of the high-temperature n- and p-type segments, the cold-side junction temperature and the load resistance applied to the couple, considering a fixed hot-side junction temperature, fixed per-couple heat input, and desired output voltage. To this end, computationally-inexpensive methods that optimize segmented unicouples are presented and compared. These methods include physics-based algorithms that dynamically reduce the design space when nonviable configurations are found, implementation of Golden Section Search (GSS) algorithm when uni-modal behavior is observed for a specific degree of freedom, and successive design space refinement. When using both GSS and successive design space refinement algorithms, an optimum geometry was found with 5,755 times fewer solver calls in comparison to the conventional parametric study without any loss of fidelity. This comparison indicates the proposed optimization methods are robust and accurate, while also drastically reducing the computation time to find the optimum unicouple configuration that maximizes system-level power output. These methods allow for exhaustive trade studies to be conducted of newly proposed heat sources, converter materials and designs, and heat exchange systems.

KEY WORDS: radioisotope thermoelectric generator, radioisotope power systems, thermoelectric converter, deep-space power generation

INTRODUCTION

Radioisotope thermoelectric generators (RTGs), a type of radioisotope power systems (RPS), have a long-standing history spanning nearly half a century of providing reliable thermal energy and electrical power to deep space probes [1]. High-efficiency thermoelectric materials, lightweight system designs, and reliable energy production are crucial for RTGs to be successful in completing their deep-space missions [2–4]. In terms of material selection, the performance of two independent thermoelectric materials, denoted

*Corresponding Matthew M. Barry: matthew.michael.barry@pitt.edu
DOI: http://dx.doi.org/10.1615/TFEC2022.aes.040925

as n- and p-type materials, depends on the temperature gradient established across them, as well as their intrinsic thermal conversion efficiency [5]. To increase the overall performance of the thermoelectric devices (TEDs) that make up an RTG, often referred to as the converters, segmented designs are often used. In a segmented configuration, the n- and p-type legs are split as to use two different materials per leg, so each material is used over its optimum temperature range. This unicouple configuration, although allowing for higher power output and thermal conversion efficiencies in comparison to an unsegmented design, complicates the design and optimization procedure. There are methods of analyzing un-segmented and segmented designs [6, 7], but these methods require a parametric or iterative modeling approach, and have limitations when considering parasitic losses from interconnectors, contact resistances, and radiative heat transfer.

Efforts have been made to optimize segmented converter designs. El-Genk et al. [8] used global optimization methods to maximize thermal conversion efficiency of segmented skutterudite-based unicouples, and compared their performance to SiGe converters. By leveraging optimization methods and skutterudites materials, a configuration was identified that required half of the typical amount of plutonium dioxide fuel to produce the same power. Holgate et al. [9] parametrically analyzed an enhanced Multi-Mission RTG comprised of skutterudite materials and found performance improvements over the current state-of-the-art Multi-Mission RTG, namely increasing beginning and end of life power, increased specific power, and higher thermal conversion efficiencies. There is still much interest in developing RTGs with higher-efficiency materials, as well as evaluating new mission-enabling heat sources, such as the compact heat source (CPHS) [10], in an attempt to exceed a specific power of 8 [W_e/kg] and thermal conversion efficiency of 12% [11]. Analyzing new materials, heat sources and converter configurations at the system level requires trade studies, which can be computationally prohibitive due to the large number of independent variables. Thus, optimization methods are needed to quickly and accurately determine not only viable materials, but designs and heat sources.

Optimization problems are often described using the following components: an objective function $f(\vec{v})$ where $\vec{v}$ is a vector containing all of the variable inputs, as well as a set of constraints on the various components of $\vec{v}$. The goal of an optimization problem is to find the value of $\vec{v}$ such that f is minimized, given the constraints are satisfied [12]. In the present work, the value of f is inverted such that the objective of optimization becomes the maximization of f. While this is a modification against convention, inverting the value of f is a trivial operation that simplifies discussion. This formulation can be made and applied to many types of problems, and is subject to many possible solution implementations, depending on the modalities of the design space in question. One of the most notable classifications of a design space is uni-modality, or the presence of only one local maximum of f within the region of inputs that satisfy constraints. A large subset of rapid optimization algorithms, such as hill-climbing or section-search methods, are only guaranteed to find a local maximum of the objective function. If the design space for these problems is multi-modal (containing several local maxima), such algorithms are no longer guaranteed to find the true solution for the optimization problem.

In order to prove the efficacy of the proposed alternative methods of optimization, a sample five-axis design space for geometric unicouple optimization is used. The objective function in this case is the total output power of the RTG. This design space modulates n-type area, p-type area, n-and p-type low-temperature segment heights, and load resistance. Using these five parameters, as well as a unicouple fixed height and temperature boundaries, it is possible to create many possible configurations for unicouples. It is straightforward to evaluate configurations over several design axes by constructing a linear grid of configurations. While such an implementation is simple and requires no assumptions, the number of necessary solver evaluations scales exponentially with the inclusion of additional design axes or higher resolutions. The present work evaluates multiple alternative methods of optimizing the unicouple design for output power, leveraging physics-based assumptions to greatly limit the number of solver evaluations to reach the true global maximum and thus increase computational speed. These methods include linear parameter sweeps, parameter sweeps with physics-based logical checks, one-axis Golden Section Search (GSS), and successive refinement algorithms. The methodologies presented herein were instrumental in the

execution of a much larger trade study performed by Durka et al. [13], which used a GSS-based algorithm to determine optimal RTG designs using novel heat sources and converter materials. Without the speedup provided by GSS, the optimization problem in that work would not have been computationally tractable. Because the proposed algorithms require fewer solver calls without sacrificing accuracy in the sample study, they can serve as a basis for future segmented converter design and optimization procedures, working toward achieving the National Aeronautics and Space Administration's goal of a 8 [W_e/kg] weight specific-power for RPS technology.

METHODOLOGY

In order to optimize TED performance by modulating geometric parameters, it is necessary to employ a solver capable of rapidly and accurately predicting performance. In this work, a one-dimensional thermal-electric coupled analytic model is implemented in MATLAB, described by Wielgosz et al. [14]. This model couples a thermal resistance network, which models linear unicouple elements, to a system of equations describing the non-linear effects within the thermoelectric elements. This allows for the characterization of the flow of heat through a segmented unicouple as a function of the applied load resistance, for the current develops implicitly with the solution. In doing such, interfacial temperatures are able to be resolved, allowing for the further consideration of additional parasitic losses and source terms, such as thermal and electrical contact resistances at material interfaces, and the thermal and electrical resistance of interconnectors. This method has been compared to other analytic methods as well as high-fidelity thermal-electric-coupled finite-volume models implemented in ANSYS CFX [15], and was shown to be in close agreement in the evaluation of system response quantities (SRQs) like output power, voltage, heat input and output, and thermal conversion efficiency. For the current study, thermal and electrical contact resistances are ignored, though the same optimization strategies are applicable to such models.

The solver is an iterative solution algorithm that resolves the system of governing equations, considering temperature-dependent material properties. From the conservation equation describing each interface of the segmented unicouple (hot-side junction, each intermediate junction of the n- and p-type legs, and the cold-side junction), a residual was defined, which is the remainder of the conservation equation after all terms were algebraically manipulated to be on one side of the equality. A convergence criterion of 1e-10 was set for all residuals. Additionally, the absolute error of each SRQ adhered to the same convergence criterion, with errors defined for heat input, n-type and p-type hot-junction, interface and cold-junction temperatures, Seebeck voltage and electrical current. The solver implemented an algorithm that stopped the iterative solution algorithm when a residual flat-lined at a value above the accepted criterion, the solver would stop. To determine the slope of the residual versus iteration, i.e. the slope of the residual-iteration curve, a four-point central difference scheme was cast using the five most recent maximum residual values. If the slope was below 1e-14, the residual was deemed to have flat-lined and the solver was stopped. This concept is illustrated in Fig. 1.

To execute this study, five systematic approaches were taken to solve the same design problem, with each successive approach incorporating additional physics-specific algorithms in an effort to reduce computational resources, and subsequently time to obtain a solution. The time to obtain a solution is defined in terms of number of solver calls, denoted N_{calls}. Anecdotally, the solver would require approximately 30 [ms] to obtain a converged solution, or to determine if a configuration was unsuitable. Given a study of high resolution or of a high number of parameters (on the order of one billion permutations), compute time was on the order of 30,000 core hours, making the problem intractable without high-performance computing resources.

Additionally, three constraints were imposed within the solver. In space power applications, it is necessary that converters not only produce sufficient power, but also sufficient output voltage V_{total} for the given thermal inventory. The converters within an RTG are connected electrically in series to increase the voltage output, and for redundancy, are also wired in parallel. The redundancy can manifest in a number parallelly-wired serial strings. For this analysis, two parallel strings were considered.

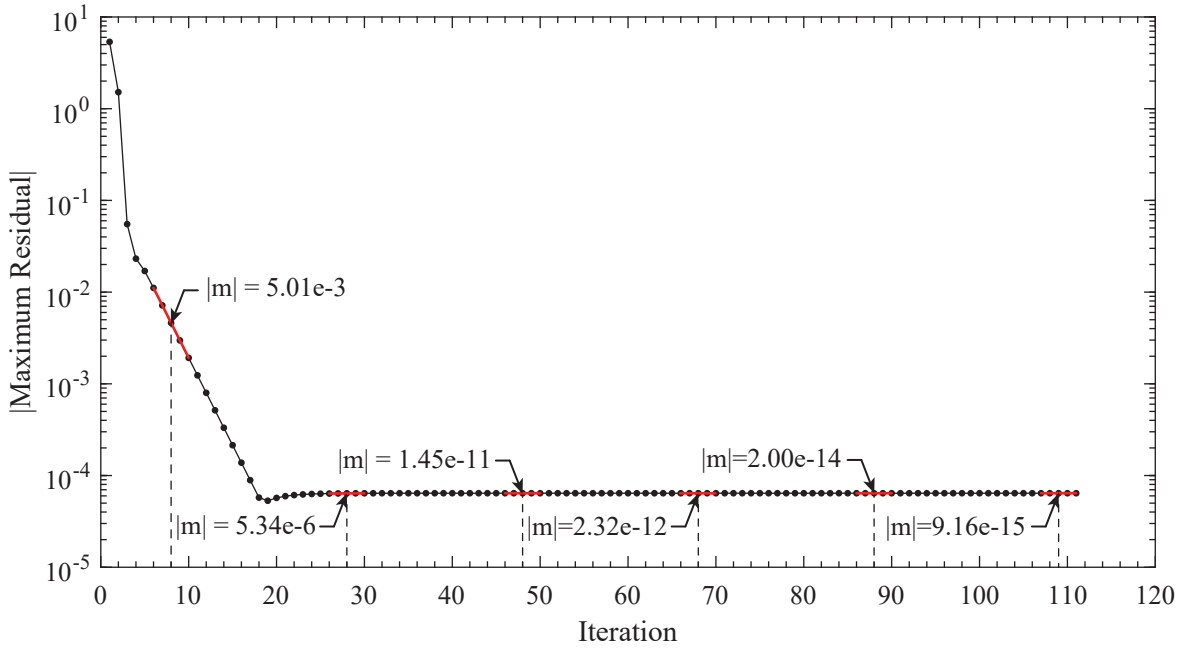

Fig. 1 Illustration of residual flat-line tracking algorithm. The red lines represent the stencil used for the four-point central difference, and the absolute value of the calculated slope via the finite-differencing method is provide for the point which the differencing was taken about.

The RTG has a given thermal inventory $Q_{total} = 4,410$ [W], a number of parallel strings $N_{\parallel,string} = 2$, and a desired voltage output $V_{total} = 30$ [V]. A unicouple is able to produce an output voltage V_{out} while receiving a heat input Q_h. Thus, an output constraint can be placed on the ratio V_{out}/Q_h between voltage output and heat input for a unicouple:

$$\frac{V_{out}}{Q_h} = N_{\parallel,string}\left(\frac{V_{total}}{Q_{total}}\right). \tag{1}$$

In order for unicouple to be deemed a viable configuration, it must be able to produce a V_{out}/Q_h greater than or equal to the quantity on the right hand side of Eqn. 1.

The second constraint is related to the maximum segment temperature of both the n- and p-type materials. The low-temperature n- and p-type segments, denoted n_{LT} and p_{LT}, have a maximum allowable temperature of 873 [K], as per the allowable limits of the MOD2 materials [13, 14]. If the interfacial temperature within either of the n_{LT} or p_{LT} segments exceeds the established limits, the solution is considered invalid. The volts per heat and maximum low-temperature segment temperature constraints are enforced after the model converges. If the model violates either or both constraints, all SRQs are set to a value zero for that particular configuration.

If a solution is valid with respect to the two constraints discussed, the number of unicouples $N_{couples}$ required to produce the desired system-level voltage, considering the number of parallel strings, is calculated using the following formula:

$$N_{couples} = N_{\parallel,string}\left(\frac{V_{total}}{V_{out}}\right). \tag{2}$$

Considering the required number of couples as described by Eqn. 2, and an assumed packing density of 0.9, the total converter cross-sectional area can be calculated. If the converters were unable to fit within the existing

RTG architecture [1], the solution was deemed impracticable and omitted. This constraint was considered sufficient for system-level modeling purposes.

Lastly, solver re-initialization was utilized to decrease number of iterations required to reach convergence without jeopardizing accuracy. For the first solver execution, the initial system of equations dictating unicouple performance was initialized with reasonable values. Once a solution was obtained, the values defining the intermediate temperatures (i.e. non-Dirichlet boundary conditions) were used to initialize the next solver call within the sequence. The order through which the independent variables were evaluated was done in a manner to capitalize on the ability to initialize the system of equations near that of the solution. With the establishment of the baseline algorithm and constraints, each modeling method is presented and described in the following subsections.

2.1 Parametric Study

The simplest approach for finding the optimum unicouple configuration that maximizes output power is a full parametric study. In such a study, each independent variable is swept through its predefined range, while every other variable was held invariant. While such a method is easy to implement and requires few assumptions about the design space, the number of necessary solver calls scales exponentially with the increase in resolution and additional independent variables. Although being computationally expensive, this procedure provides a benchmark set of data for which solutions obtained via faster methods can be compared against, both in terms of obtained solution and number of solver calls. The range of the design space used in the all methods is provided in Tab. 1, and a schematic of the unicouple is shown in Fig. 2. The lower and upper bounds provide the limits for the areas of the n- and p-type materials, the lengths of the low-temperature n- and p-type segments per the total unicouple leg length, and the range of load resistance values. The number of increments within the defined ranges, N_Δ, is provided for the parametric methods. The number of increments used within the successive refinement algorithm (Step 1 and Step 2) are also provided. It is noted that Step 2's resolution's is an effective resolution with respect to the lower and upper bounds and number of grid points, as well be discussed in Sec. 2.4. The total length of the unicouple is fixed at 9 [mm]. The cold- and hot-junction temperatures are fixed at 550 [K] and 1,273 [K], respectively. The materials in this analysis are proprietary materials from the National Aeronautics and Space Administration's Jet Propulsion Laboratory [14], but the process applied in the present work is applicable for any set of materials with sufficient compatibility for a segmented unicouple configuration.

Table 1 Input parameter specification. The five independent parameters are described in terms of their lower and upper bounds, and the number of increments (N_Δ) used for the parametric studies, and the successive refinement methodology. The successive refinement methodology has N_Δ defined as the effective resolution in terms of the Step 1 and Step 2 design spaces.

	Bound		N_Δ		
			Parametric	Successive Refinement	
Parameter	Lower	Upper		Step 1	Step 2
A_n [cm^2]	0.02	0.5	15	8	15
A_p [cm^2]	0.02	0.5	15	8	15
$L_{n,LT}/L_{total}$ [-]	0.2	0.8	25	13	25
$L_{p,LT}/L_{total}$ [-]	0.2	0.8	25	13	25
R_{load} [Ω]	0.001	10	10,001	5,001	10,001

As seen from Tab. 1, load resistance has the largest number of steps. This is due to two reasons. The first is considering an incredibly large geometric design space, there is a large range of internal resistance values that manifest from a variety of area and length combinations. To ensure that no configuration was arbitrarily omitted, a large design space for R_{load} was considered. Secondly, the performance predictions of the

unicouple are highly sensitive to the applied load resistance. The change between load resistance values must be sufficiently small to be able to accurately model the performance of the device.

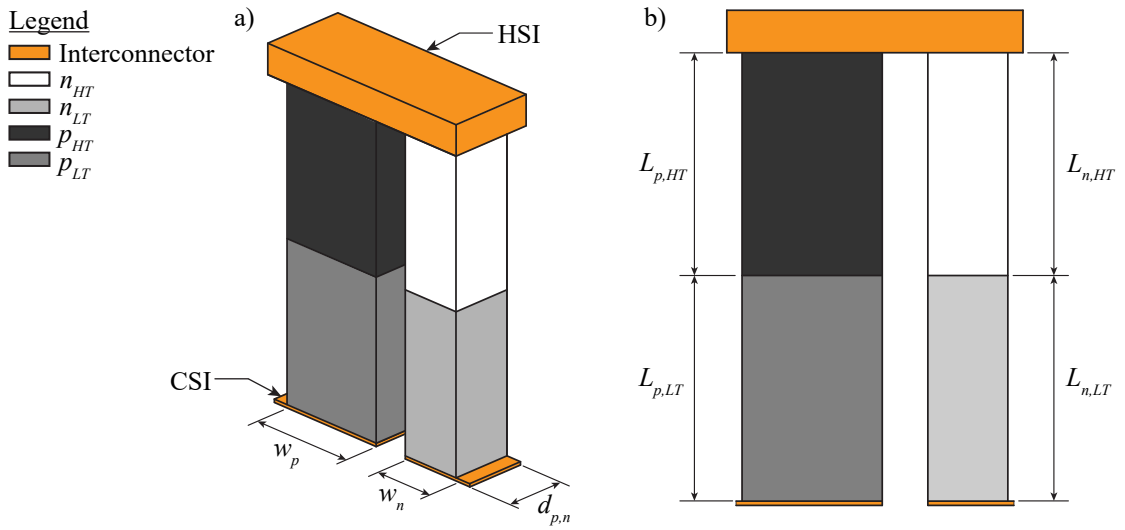

Fig. 2 Schematic of segmented unicouple, with hot- and cold-side interconnectors (HSI and CSI, respectively). Note the width of the n- and p-type materials, w_n and w_p, are variable, for a fixed p- and n-type depth, $d_{p,n}$. The length of the high-temperature and low-temperature n- and p-type segments are all variable.

2.2 Parametric Study with Conduction and Load Resistance Logic

Recognizing that sweeping load resistance constituted the majority of solver calls, two logical checks were implemented. The first was a conduction check. To implement a conduction check, the load resistance was swept from the highest to lowest value, and the low-temperature segment lengths of the n- and p-type materials were incremented from the lowest to highest values in their array definitions.

If the n- or p-type low-temperature segment interfacial temperatures exceeded the allowable limit of 873 [K], or the n- and p-type high-temperature segment hot-side temperatures exceeded the allowable limit of 1,273 [K] for the highest load resistance, i.e. a near-conduction only situation, then two things occurred. First, the configuration in consideration was deemed nonviable and all SRQs were set to zero. Second, since it is expected that any further increase in segment height would cause an increase in interfacial temperatures from the already-nonviable point, the remaining segment height for that sweep are skipped. A further increase in the n- and p-type low-temperature segment lengths would cause further violations of the interfacial temperature limit under the conduction-only situation.

The second logical check was associated to the load resistance. If the configuration of interest passed the conduction logical check, the load resistance was incrementally decreased. As R_{load} decreased, if a situation arose where any of the temperature constraints were violated, the SRQs of that configuration, as well as that configuration with lesser load resistances, were all set to zero, and the load resistance sweep was terminated. A further decrement in load resistance only increases the interfacial temperatures due to an increase in heat generation terms, so those other configurations need not be tested.

2.3 Parametric Study using GSS

To reduce the number of unique configurations evaluated, specifically load resistance, the Golden Section Search (GSS) algorithm was implemented to more quickly determine the optimal load resistance for a given geometry. The GSS algorithm is able to find a maximum within a specified interval in logarithmic time, through successive interval refinement [16]. This is done by evaluating the function, in this case power output,

at two unique load resistance values , e.g. $R_{load,1}$ and $R_{load,2}$, which define three intervals, $\Delta x_{start,1}$, $\Delta x_{1,2}$ and $\Delta x_{2,end}$, respectively, as shown in Fig. 3 a). When comparing the values, say $P_{out,1} > P_{out,2}$, it is seen the maximum must not lie within $\Delta x_{2,end}$. The process of evaluating the function is repeated, this time using the load resistances $R_{load,start}$ and $R_{load,2}$ as lower and upper bounds, with defining an intermediate load resistance value between the two defined bounds, as shown in Fig. 3 b). This method requires the evaluated function containing only one local maximum such that the section-search locates the proper peak.

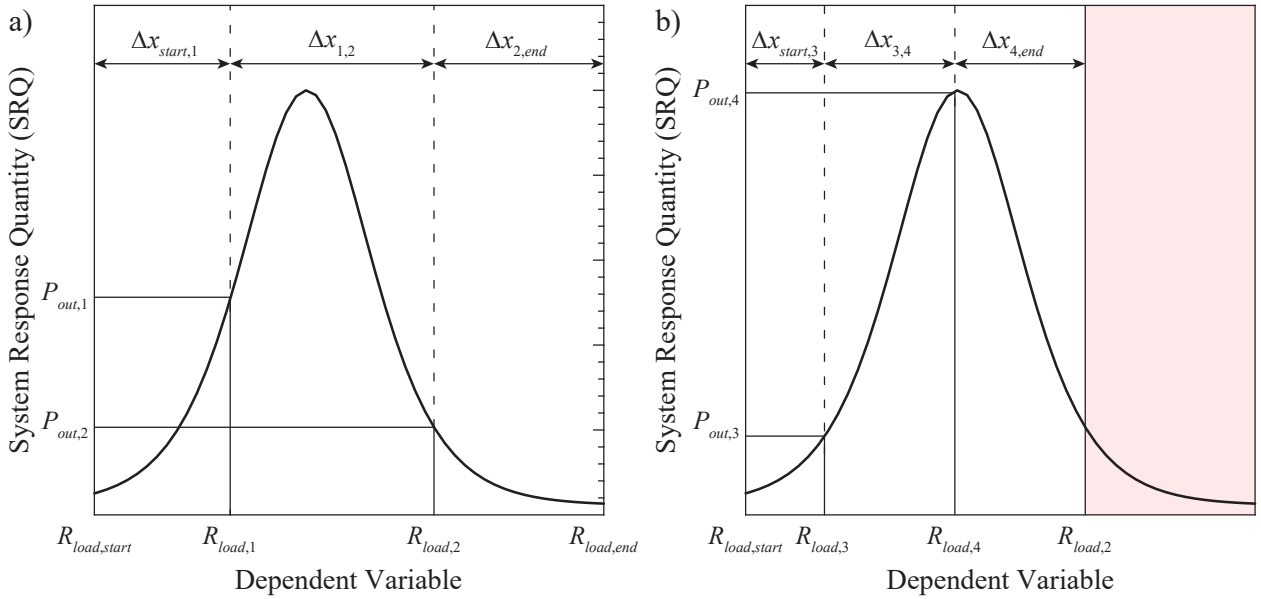

Fig. 3 Representation of a) the first step of the GSS algorithm using bounds $R_{load,start}$ and $R_{load,end}$, and b) the second step using the updated bounds $R_{load,start}$ and $R_{load,2}$ while searching for the global maximum. The red shaded region indicates the portion of the design space no longer considered.

2.4 Successive Refinement

The final method implemented was a successive refinement algorithm. As opposed to evaluating the entire design space using the increments as defined in Tab. 1, the number of the increments used were decreased, creating a coarse design space, denoted as Step 1 in Tab. 1. The coarse design space was evaluated, and the results parsed to find the region for where the global maximum occurred. Taking the lower and upper bound of each of the independent variables, a refined design space was created, once again using a relatively few number of increments to design the array of variables, as denoted by Step 2 in Tab. 1. This process can further be repeated until the percent difference of the desired SRQ(s) between successive refinements is within acceptable limits. Successive refinement was applied to the method described in Sec. 2.1, which will be denoted as Method 2.4 a), and additionally to the method described in Sec. 2.3, which will be denoted as Method 2.4 b). A summary of all methods is presented in Tab. 2, where each method is denoted by the corresponding section heading number under which the method was described.

RESULTS AND DISCUSSION

Table 3 provides the predicted power output of the converter for each of the aforementioned methods, as well as the required number of solver calls and normalized solver calls for each method. Additionally, the optimal configurations revealed by each method given the same objective and constraints are provided. Lastly, the primary SRQs, on a per-unicouple basis, are given. Note that Q_h is the heat input, $T_{n,if}$ and $T_{p,if}$ are the interfacial segment temperatures between the low- and high-temperature materials in the n- and p-type legs, respectively, and R_{int} is the internal resistance of the unicouple.

Table 2 Summary of modeling methods.

Method	Solver Re-initialization	Residual Tracking	Conduction Check	R_{load} Check	GSS	Successive Refinement
2.1	Yes	Yes	No	No	No	No
2.2	Yes	Yes	Yes	Yes	No	No
2.3	Yes	Yes	No	No	Yes	No
2.4 a)	Yes	Yes	No	No	No	Yes
2.4 b)	Yes	Yes	No	No	Yes	Yes

First and foremost, all methods predict the same system-level power output of 562.5 [W], with the only difference being Method 2.3, which utilized GSS, predicting a power output 0.13% higher. While the tolerance of the GSS algorithm was set to be the same as the grid size from the linear sweep, the GSS algorithm does not return a result on a corresponding grid line. As such, the difference in power is expected. Power output predictions are highly sensitive to changes in the specified load resistance, and using a finer resolution in the load resistance design space provides the ability to find the true maximum. The geometry that maximized the power output was found to be the same for all methods except Method 2.3, which predicted larger $L_{n,LT}$ and $L_{p,LT}$ values and a lesser A_p value. These geometrical changes resulted in a lesser heat input and higher n- and p-type interfacial segment temperatures. The increase in interfacial temperatures led to an increase in internal resistance and load resistance, leading to a lesser output voltage and unicouple power output. With a lesser voltage, more unicouples were required to meet the voltage requirement of 30 [V]. Therefore, the total power imperceptibly increased despite the slight decrement in per-unicouple power.

Table 3 Results obtained via a full parametric study (Method 2.1), a parametric study with conduction and load resistance logic (Method 2.2), GSS (Method 2.3, and successive refinement applied to a full parametric study (Method 2.4 a)) and GSS (Method 2.4 b)).

Method	2.1	2.2	2.3	2.4 a)	2.4 b)
Total Power (P_{total}) [W]	562.5	562.5	563.2	562.5	562.5
Couples ($N_{couples}$)	380	380	384	380	380
Solver Calls (N_{calls})	1,406,390,625	801,585,042	3,253,470	54,093,941	244,341
$\|\|N_{calls}\|\|$	1.0000	0.5700	0.0023	0.0385	0.0002
$L_{n,HT}$ [mm]	3.8250	3.8250	3.6000	3.8250	3.8250
$L_{n,LT}$ [mm]	5.1750	5.1750	5.4000	5.175	5.1750
$L_{p,HT}$ [mm]	3.6000	3.6000	3.3750	3.6000	3.6000
$L_{p,LT}$ [mm]	5.4000	5.4000	5.6250	5.4000	5.4000
A_n (1e-1) [cm^2]	2.257	2.257	2.257	2.257	2.257
A_p (1e-1) [cm^2]	3.971	3.971	3.629	3.971	3.971
Q_h [W]	11.636	11.636	11.456	11.636	11.636
$T_{n,if}$ [K]	856.068	856.068	872.524	856.068	856.068
$T_{p,if}$ [K]	821.413	821.413	840.740	821.413	821.413
R_{int} (1e-2) [Ω]	1.206	1.206	1.229	1.206	1.206
R_{load} (1e-2) [Ω]	1.670	1.670	1.681	1.670	1.670
V_{out} (1e-1) [V]	1.586	1.586	1.570	1.586	1.586
P_{out} [W]	1.480	1.480	1.467	1.480	1.480

It is seen within Tab. 3 that the maximum power does not occur when the load resistance is equal to the internal resistance of the unicouple. One must recall both the voltage and temperature constraints applied.

While a further decrease of load resistance applied to the optimal configuration might increase power further, the design then exceeds allowable interfacial temperatures, or does not meet the required system-level output voltage. This also shows the value of sweeping load resistance to capture optimal designs where $R_{load} \neq R_{int}$.

The impetus of this study was not to quantify the unicouple and system-level performance, but rather determine which method or methods would reliably find the optimum configuration while minimizing the number of solver calls, and thus the computational requirement. The full parametric study incurred the largest number of solver calls, for it had to evaluate the entirety of the design space at the full resolution provided. By incorporating a conduction and load resistance check, the number of solver calls decreased 43% with respect to the simple study. By using previous solutions to determine and skip known, invalid configurations, the number of necessary solver calls decreased substantially while still discovering the optimum configuration. The conduction check is illustrated in Fig. 4 where for a set maximal load resistance and n- and p-type areas, an increment in the n- or p-type low-temperature segment height caused a further violation of the interfacial temperature limits. It is seen in Fig. 4 a) that once the the ratio of $L_{n,LT}/L_{total}$ exceeded 0.6, any further increment in $L_{n,LT}$ led to the interfacial temperature continuously exceeding the prescribed limit of 873 [K], and thus the assumption of setting SRQs associated with the remainder of the $L_{n,LT}$ design space to zero is valid. The same is seen in Fig. 4 b), where once the ratio of $L_{p,LT}/L_{total}$ exceeded 0.675, the p-type interfacial temperature limit was exceed with any further increase in $L_{p,LT}$.

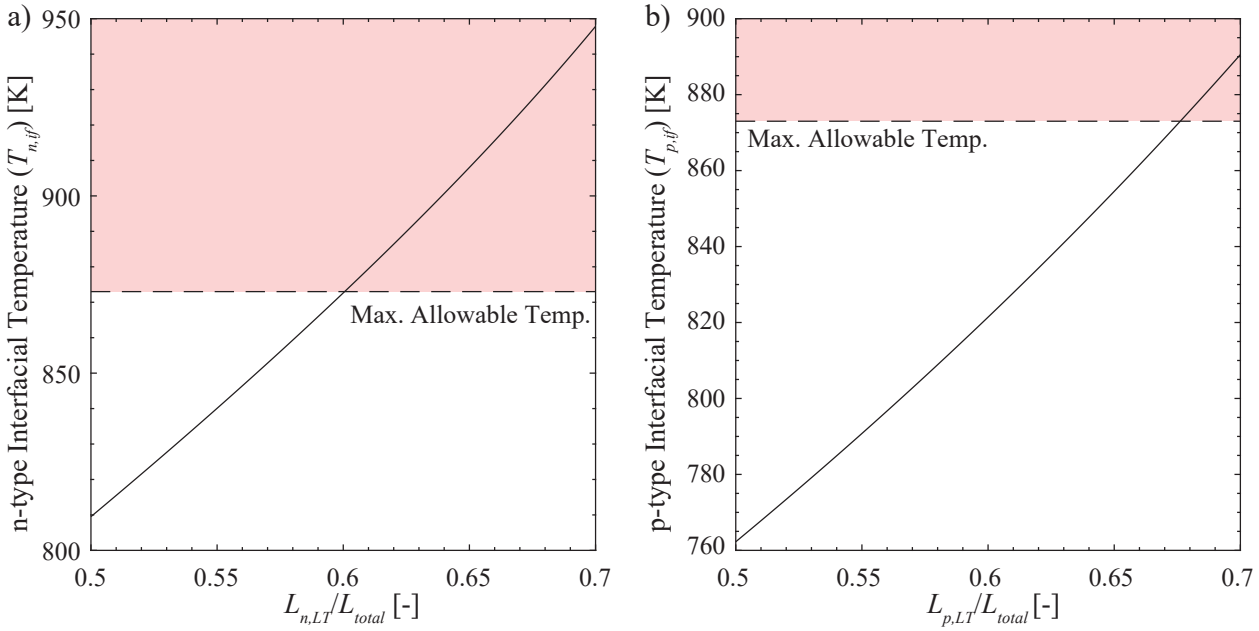

Fig. 4 Illustration of elimination of non-viable geometries via the conduction check algorithm when interfacial temperature were violated with increasing a) L_{nLT} and b) L_{pLT} values. The red shaded regions indicates a violation of the interfacial temperature limit. The geometry modelled is a modified version of the optimal case for Method 2.1 shown in Tab. 3.

Similarly, the load resistance check was able to reduce the computational requirements, as illustrated in Fig. 5. With a decrement of load resistance, the interfacial temperatures of the n- and p-type materials would increase, given fixed cross-sectional areas and lengths. For this example, once the load resistance fell below a value of approximately 6 [mΩ], the n-type interfacial temperature exceeded the allowable limit for the demonstrable configuration. Any further decrement in the load resistance would lead to a continual violation of the interfacial temperature limit for the n-type material and led to an eventual violation of the p-type interfacial temperature limit. Thus, the assumption of setting all remaining SRQs within the remainder of load resistance design space for that particular geometric configuration to zero is valid.

Through implementing the GSS method in lieu of both the conduction and load resistance check, the second-most marked improvement of decreased solver calls was obtained. Via the use of Method 2.3, the number of solver calls decreased 99.59% in comparison to Method 2.2 and 99.77% in comparison to Method 2.1, with no loss of fidelity in predicting the geometry and load resistance values to maximize power output. This significantly pronounced decrement in the number of solver calls was because of the logarithmic runtime of the GSS algorithm with respect to load resistance resolution, which allows the optimal load resistance per configuration to be found within tens of solver evaluations instead of 10,001 (for the prescribed resolution).

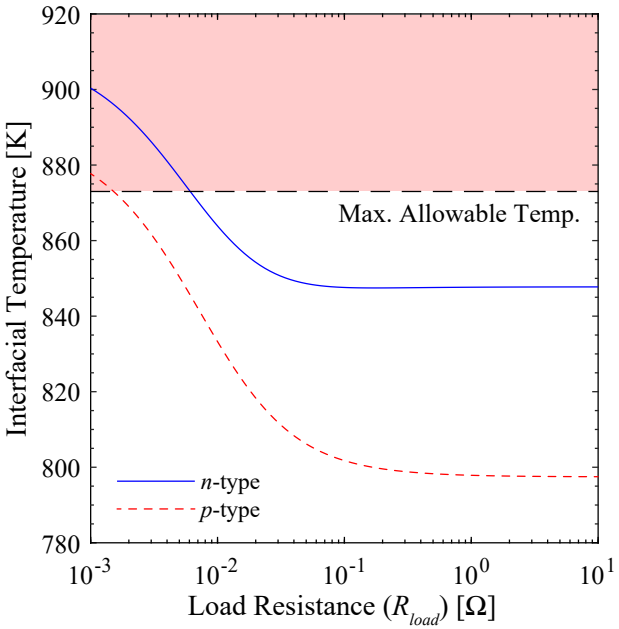

Fig. 5 Load resistance check algorithm and elimination of non-viable operating points, as indicated by the red shaded region.

Applying a successive refinement scheme to the full parametric study and GSS, i.e. Methods 2.4 a) and b), had even greater impacts on reducing the number of solver calls. Using successive refinement alone, without the incorporation of conduction or load resistance checks, reduced the number of times the solver was executed by 96.15% versus the simple sweep. This reduction is comparable to the application of GSS algorithm on the full parametric study, but exhibits a normalized number of solver calls an order magnitude higher than that of GSS. The greatest reduction in the number of times the solver was called was achieved by using a combination of a successive refinement scheme and the GSS algorithm. Method 2.2 b) achieved a 99.98% reduction in solver calls by using GSS to quickly resolve load resistance and successive refinement to limit the necessary number of GSS sweeps necessary. The application of the successive refinement algorithm is shown in Fig. 6.

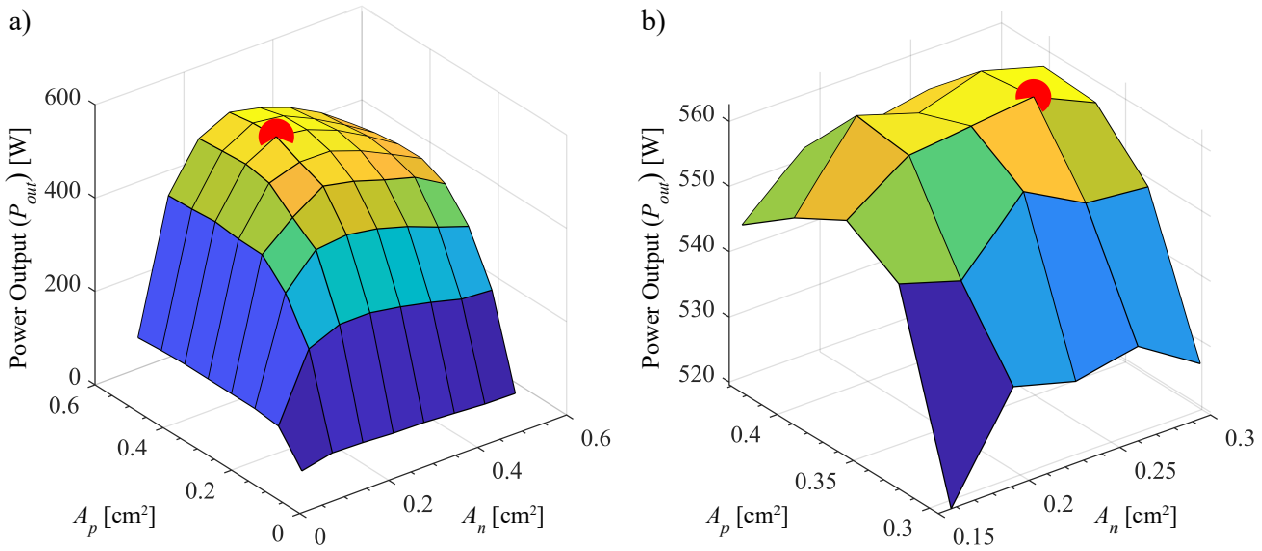

Fig. 6 Illustration of successive refinement algorithm using a) a coarse domain (Step 1) in which the global maximum is identified (red dot), and b) a subsequent finer domain (Step 2), with identification of global maximum (red dot).

By using a coarse domain, as shown in Fig. 6 a), a global maximum can quickly identified, as shown by the red dot. This is denoted as Step 1 of the process. Once the global maximum is identified, the lower and upper bounds are redefined in terms of the nearest grid points. Using Fig. 6 a) as an example the lower and upper bounds for A_n are redefined as 0.1571 and 0.29473 [cm^2], respectively, and those for A_P as 0.2943 and 0.4314 [cm^2], respectively. As seen in Fig. 6 b), these values serve as the new global bounds, and refinement of the new domain occurs. This is denoted as Step 2 of the process. Thus, a new global maximum is found in the region of interest.

CONCLUSIONS

Several methods for conducting trade studies of thermoelectric converters within radioisotope thermoelectric generators are presented. These methods include computationally-expensive, conventional full parametric studies, as well as computationally-inexpensive methods. The full parametric study provided both benchmark data in terms of optimum unicouple and converter configurations, as well as the number of solver calls. The computationally inexpensive methods leveraged physics-based logical algorithms to curtail the design space, the use of GSS algorithms to drastically reduce the evaluation of large design spaces where pertinent system response quantities exhibited uni-modal behavior, as well as successive refinement algorithms that dynamically updated both the bounds and resolution of the design space. The motivation of developing these methods was to reduce the number of solver calls without compromising the fidelity of the solution. The assumptions underpinning such computationally-inexpensive methods are demonstrated to be valid, for the solution of the optimum unicouple configuration agrees with the bench-mark data. It was found through the use of both the GSS and successive refinement algorithms that the number of solver calls was reduced by a factor of 5,755 in comparison to the full parametric study, yet the same optimum unicouple configuration in terms of geometry and operating point was found. These proposed modeling methodologies make trade studies computationally tractable, allowing for the analysis of novel heat sources, novel thermoelectric materials, and converter designs.

ACKNOWLEDGMENTS

This research was carried out at the Jet Propulsion Laboratory, California Institute of Technology, under a contract with the National Aeronautics and Space Administration, CL#: 21-5714, and at the University of Pittsburgh. Computational resources and support were provided by the Center for Research Computing (CRC) at the University of Pittsburgh.

The remainder of this page is intentionally left blank.

NOMENCLATURE

Variables

A	area	(cm^2)
d	depth	(m)
f	objective function	
L	length	(m)
n	n-type	(-)
N	number	(-)
p	p-type	(-)
P_o	power output	(W)
Q	heat	(W)
R	electrical resistance	(Ω)
T	temperature	(K)
$\vec{v}$	variable input vector	
V	voltage	(V)
w	width	(m)
W	power	(W)

Subscripts and Superscripts

1, 2, 3	indices	$load$	load
$calls$	solver calls	LT	low-temperature
$couples$	couples	n	n-type
e	electric	out	output
h	hot-side	$\|$	parallel
if	interfacial	p	p-type
int	internal	$string$	strings
HT	high-temperature	$total$	total

Greek Letters

Δ	increment	(-)

Acronyms

CSI	cold-side interconnector	RTG	radio-isotope thermoelectric generator
GSS	Golden Section Search	SRQ	system response quantity
HSI	hot-side interconnector	TED	thermoelectric device
RPS	radio-isotope propulsion systems		

REFERENCES

[1] G. Bennett, J. Lombardo, R. Hemler, G. Silverman, C. Whitmore, W. Amos, E. Johnson, A. Schock, R. Zocher, T. Keenan, *et al.*, "Mission of daring: the general-purpose heat source radioisotope thermoelectric generator," in *4th International Energy Conversion Engineering Conference and Exhibit (IECEC)*, p. 4096, 2006.

[2] M. S. El-Genk, H. H. Saber, and T. Caillat, "Efficient segmented thermoelectric unicouples for space power applications," *Energy Conversion and Management*, vol. 44, pp. 1755–1772, 2003.

[3] R. O'Brien, R. Ambrosi, N. Bannister, S. Howe, and H. V. Atkinson, "Safe radioisotope thermoelectric generators and heat sources for space applications," *Journal of Nuclear Materials*, vol. 377, no. 3, pp. 506–521, 2008.

[4] C. S. Matthes, D. F. Woerner, T. J. Hendricks, J.-P. Fleurial, K. I. Oxnevad, C. D. Barklay, and J. F. Zakrajsek, "Next-generation radioisotope thermoelectric generator study," in *2018 IEEE Aerospace Conference*, pp. 1–9, IEEE, 2018.

[5] T. Ursell and G. Snyder, "Compatibility of segmented thermoelectric generators," in *Twenty-First International Conference on Thermoelectrics, 2002. Proceedings ICT'02.*, pp. 412–417, IEEE, 2002.

[6] G. J. Snyder and T. S. Ursell, "Thermoelectric efficiency and compatibility," *Physical review letters*, vol. 91, no. 14, p. 148301, 2003.

[7] G. J. Snyder, "Application of the compatibility factor to the design of segmented and cascaded thermoelectric generators," *Applied physics letters*, vol. 84, no. 13, pp. 2436–2438, 2004.

[8] M. S. El-Genk, H. H. Saber, and T. Caillat, "Efficient segmented thermoelectric unicouples for space power applications," *Energy Conversion and Management*, vol. 44, no. 11, pp. 1755–1772, 2003.

[9] T. C. Holgate, R. Bennett, T. Hammel, T. Caillat, S. Keyser, and B. Sievers, "Increasing the efficiency of the multi-mission radioisotope thermoelectric generator," *Journal of Electronic Materials*, vol. 44, no. 6, pp. 1814–1821, 2015.

[10] D. Woerner, S. Johnson, J.-P. Fleurial, S. Howell, B. Bairstow, and M. Smith, "Radioisotope heat sources and power systems enabling ocean worlds subsurface and ocean access missions," *Bulletin of the American Astronomical Society*, vol. 53, no. 4, p. 322, 2021.

[11] N. Aeronautics and S. Administration, "Nasa technology roadmaps, ta 3: Space power and energy storage," May 2015.

[12] R. Bellman, *Mathematical optimization techniques*. Univ of California Press, 1963.

[13] M. Durka, J.-P. Fleurial, S. Wielgosz, S. Riley, M. Barry, D. Woerner, B. Barstow, F. Drymiotis, and B. Nesmith, "A novel high-performance mission-enabling multi-purpose radioisotope heat source," in *2022 IEEE Aerospace Conference*, IEEE, 2022.

[14] S. Wielgosz, K. Yu, A. Mamoozadeh, F. Drymiotis, M. Durka, B. Nesmith, J.-P. Fleurial, and M. Barry, "Mathematical and numerical modeling of next-generation segmented thermoelectric converters with electrical and thermal contact resistances." Unpublished.

[15] S. Wielgosz, C. Clifford, K. Yu, and M. Barry, "Fully-coupled thermal-electric modeling of thermoelectric generators." Unpublished.

[16] J. Kiefer, "Sequential minimax search for a maximum," *Proceedings of the American mathematical society*, vol. 4, no. 3, pp. 502–506, 1953.